SAE INTERNATIONAL

2017-24-0032

Published 09/04/2017

Evaluation of Wall Heat Flux Models for Full Cycle CFD Simulation of Internal Combustion Engines under Motoring Operation

Gilles Decan and Stijn Broekaert
Ghent University

Tommaso Lucchini and Gianluca D'Errico
Politecnico di Milano

Jan Vierendeels and Sebastian Verhelst
Ghent University

CITATION: Decan, G., Broekaert, S., Lucchini, T., D'Errico, G. et al., "Evaluation of Wall Heat Flux Models for Full Cycle CFD Simulation of Internal Combustion Engines under Motoring Operation," SAE Technical Paper 2017-24-0032, 2017, doi:10.4271/2017-24-0032.

Abstract

The present work details a study of the heat flux through the walls of an internal combustion engine. The determination of this heat flux is an important aspect in engine optimization, as it influences the power, efficiency and the emissions of the engine. Therefore, a set of simulation tools in the OpenFOAM® software has been developed, that allows the calculation of the heat transfer through engine walls for ICEs. Normal practice in these types of engine simulations is to apply a wall function model to calculate the heat flux, rather than resolving the complete thermo-viscous boundary layer, and perform simulations of the closed engine cycle. When dealing with a complex engine, this methodology will reduce the overall computational cost. It however increases the need to rely on assumptions on both the initial flow field and the behavior in the near-wall region. As the engine studied in the present work, a Cooperative Fuel Research (CFR) engine, is a simple single cylinder pancake engine, it was possible to implement more complex and numerically demanding methodologies, while still maintaining an acceptable computation time. Both closed and full cycle simulations were therefore performed, for which the heat flux was calculated by both implementing various wall function models and by resolving the complete thermo-viscous boundary layer. The results obtained from the different kind of simulations were then compared to experimental heat flux data, which was measured using a thermopile type heat flux sensor in different locations in the CFR engine. By comparing the results from the different types of simulations, a performance evaluation of the used methodology could be carried out. It was found that the heat flux obtained by resolving the thermo-viscous layer was accurate compared to experiments, while the wall functions were not able to correctly capture the heat flux. Full cycle simulations resulted in a slightly improved result, especially when resolving the boundary layer, but due to the increased computational cost, this method does not seem beneficial.

Introduction

Due to increasingly stringent emission legislations and the increasing social awareness to improve engine efficiency and reduce the exhaust of harmful emissions, current engine research is focused on developing and improving new engine technologies. Heat transfer calculations play an important part in the optimizing strategy of internal combustion engines, as it influences the engine efficiency, power output and emissions [1, 2, 3, 4, 5, 6, 7, 8]. Currently, research is focused on two aspects: simulation strategies on the one hand, to predict the heat flux in an accurate manner and aid in reducing the time-consuming approach of only relying on experiments; and on the other hand, developing new measurements tools to accurately capture the heat flux and other experimental parameters, as an aid for optimization as well as validation of these simulation strategies.

An example of such a measurement tool is the Thin Film Gauge sensor presented in the research of De Cuyper et al. [5,9]. This type of sensor was mounted at various locations inside an engine cylinder and used by Broekaert et al. [3] and De Cuyper et al. [6] to capture the wall temperature and calculate the wall heat flux. Such results can then be used to develop new heat transfer models or evaluate existing models and validate and optimize them for different engine technologies.

Another interesting tool are PIV-measurements of the flow field of an optically accessible engine, as performed by Koehler et al. [10], Müller et al. [11] and Ma et al. [12,13]. These measurements can capture the flow field in the entire engine. For closed cycle CFD

simulations these images can determine the flow field at inlet valve closing time (IVC), which can be imposed to the start of the simulation. PIV-images can also be used to validate numerical methods of engine simulations, as is done by Ma et al. [12,13], where they validate their wall modeling technique with these PIV-measurements of the wall flow field.

As already briefly mentioned, experimental results can be useful for the validation and the development of modeling techniques. Concerning heat transfer modeling, Annand [14] and Woschni [15] were the first ones to develop an empirical correlation for the determination of the heat flux through the cylinder walls of a diesel engine. Alkidas [16,17] did the same for a gasoline engine. As different engine operating principles emerge, these and other developed correlations [18,19] need to be validated for the engine operation. As was demonstrated by Broekaert et al. [3], the current correlations are not able to correctly predict the heat flux for a complex operation such as HCCI combustion. Other tools besides these heat flux correlations are necessary to calculate the heat flux in a numerical way and aid the engine optimization process.

A different numerical approach of calculating the heat flux through the engine walls, is to perform Computational Fluid Dynamics (CFD) simulations of the engine operation. This method is increasingly being used, as computational power increases, allowing a more efficient and faster simulation of complex engine geometries. The general approach in this type of heat flux calculations is to apply a thermal wall function at the boundaries, not resolving the thermo-viscous near-wall region and thus reducing the numerical expenses. Different wall models were developed, with the most important ones those of Launder and Spalding [20], Huh et al. [21], Han and Reitz [22], Angelberger et al. [23] and Rakopoulos et al. [24]. They differ by accounting for variable density or other variable thermodynamic properties, or by not neglecting the pressure work term from the energy equation. Rakopoulos et al. [24] applied all mentioned wall models to their engine simulations, to investigate and compare their performance. They found acceptable results for the model developed by Han and Reitz [22] and the one by Rakopoulos et al. [24], while finding inaccurate results for the others. On the other hand however, Nijeweme et al. [8] and Reitz et al. [25] note that this wall model approach always under-predicts the heat flux, and that other methods are necessary to correctly calculate the heat flux through engine walls. Only in some cases, accurate results are achieved with these wall function models [26].

Nijeweme et al. [8] and Ma et al [13] implemented, besides a few wall models, also a non-equilibrium method. Unlike the wall model approach, where the transient and convection terms from the energy equation are always neglected, these terms were accounted for in this method. They reported an improved prediction of the wall heat flux when using the non-equilibrium method. Additionally, Ma et al. [13] were able to compare the flow field in the near-wall region with experimental PIV-images. These also showed a better simulation result when using this non-equilibrium method than when applying a wall function.

In this work, both approaches, namely a wall model and a non-equilibrium formulation, were used, to allow a complete comparison between different methods. The OpenFOAM® software was used to conduct closed cycle simulations, with all the mentioned wall models as well as with a method that resolves the near-wall region. The flow field at IVC is however not known, as for the used CFR engine, no experimental flow field measurements were available. For the same CFR engine, Rakopoulos et al. [27,28] create a swirling flow at IVC to start their calculation, based on the assumption of a swirl ratio of 1.5. As the CFR is a fairly simple engine, with unshrouded valves and straight inlet and exhaust ducts, this low swirl ratio seems accurate and was therefore also used during this research.

However, to achieve more accurate results, also 3D full cycle simulations were performed, which would automatically result in knowledge of the flow field at IVC. Both the wall function approach and this non-equilibrium method were applied to these full cycle simulations. By comparing the obtained results with those from the closed cycle simulations, this also allowed an investigation of the importance of the flow field for the prediction of the wall heat flux.

In the remainder of the paper, the experimental setup is discussed followed by the used numerical methodology and models. A short discussion on the different approaches is given, together with a brief derivation of certain aspects of the model. A more detailed discussion on the different modeling techniques can be found in the discussed specific literature on these models. Results from both closed and full cycle simulations, using these different approaches, are then presented and compared, with the aid of experimental results. The performance of the different methods and models was evaluated, which is discussed afterwards. The findings and conclusions are then briefly summarized.

Experimental Setup

Measurements of the wall heat flux during motored operation were available from a Waukesha Cooperative Fuel Research or CFR engine. This is a simple single-cylinder pancake engine, originally used for octane number rating but now mainly used for research due to its simple geometry and variable engine speed and compression ratio. The full engine geometry consists of a single cylinder, straight and symmetric intake and exhaust ducts and 2 symmetric unshrouded valves. A graphical representation of a cross-section of the engine can be seen in Figure 1, where also the location of the heat flux probes is indicated. One heat flux probe is situated in the cylinder head, 29.7 mm off-center, at the position of the spark plug, which has been removed. Three other sensor locations are situated in the liner, with the center of the sensor 9 mm below the cylinder head and evenly spaced around the cylinder bore. These probes are Vatell HFM-7 sensors, which consist of a thermopile, capable of determining the heat flux, and a Resistance Temperature Detector or RTD to measure the wall temperature [4]. A Vatell AMP-6 amplifier is used to amplify the electrical output signals, which are directly correlated to the measured quantities through the calibration constants supplied by the manufacturer [4].

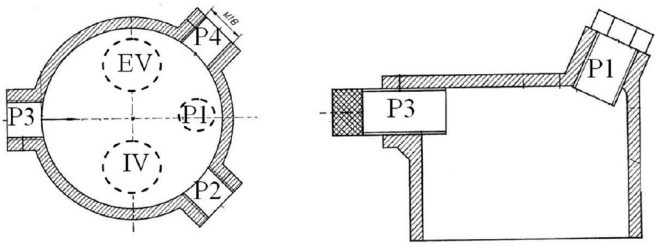

Figure 1. Graphical representation of the HFM probe locations (P1-4) in the CFR engine. EV and IV stand for exhaust and inlet valve respectively. [4]

The specifications of the engine are summarized in Table 1. As said before, engine speed and the compression ratio are variable for this CFR engine. However, during simulations, only cases with an engine speed of 600 rpm and a compression ratio of 9, 10 or 11 were studied. This is also indicated in Table 1. Additionally, valve timings are also given at 0.25 mm lift.

Table 1. Specifications of the CFR engine

Number of cylinders	1
Engine speed	600 rpm
Bore	83.06 mm
Stroke	114.2 mm
Connecting rod length	254 mm
Displacement	618.8 cm³
Compression ratio	9 – 10 – 11
Intake Valve Opening (IVO)	10° ATDC @ 0.25 mm lift
Intake Valve Closing (IVC)	29° ABDC @ 0.25 mm lift
Exhaust Valve Opening (EVO)	39° BBDC @ 0.25 mm lift
Exhaust Valve Closing (EVC)	12° ATDC @ 0.25 mm lift

Besides this CFR engine, also other engine geometries were used during the simulations. These other engines were the standard GM and the GM Triptane engine for which the geometry is described by Rakopoulos et al. [24]. The results obtained for these engines however served more as a validation of the used methods by comparing the obtained results with the results from Rakopoulos et al. [24] and less as the actual study. The CFR engine was more suited for this as an extensive experimental database was available using a contemporary and accurate sensor.

Numerical Heat Flux Calculations

Every practical Computational Fluid Dynamics problem is based on solving the continuity, momentum and energy equation for a complex geometry. Various methods exist in solving these numerically, among which are DNS, LES or RANS methods. In this research, a RANS or Reynolds Average Navier Stokes method was opted for. This is a method that averages the continuity, momentum and energy equations and therefore only solves these for the average flow field.

As only the average flow field is calculated, turbulence is not resolved and a turbulence model is necessary to close the governing equations, which means determining the turbulent terms in the equations, and model the fluctuating fields. Various turbulence models exist, among which the most popular are the k-ε model, in its standard, realizable or RNG form, and the k-ω SST model. As the focus of this work was on investigating the heat flux calculation, the most simple turbulence model was chosen, namely the standard k-ε model. Afterwards the influence of this turbulence model on the heat flux results was investigated by using the k-ω SST model, but no significant difference in the results was found.

This k-ε turbulence model incorporates a few numerical constants for which a value should be chosen. To guarantee accurate turbulence modeling, the standard values used in the OpenFOAM® software, which are also the common best-practice values, have been chosen for this study. A summary of the parameters and their values, as they have been implemented in the OpenFOAM® software, can be seen in Table 2.

Table 2. Values of parameters in the standard k-ε model

Constant	C_μ	C_1	C_2	C_3	σ_k	σ_h	σ_ε
Value	0.09	1.44	1.92	0	1.0	1.0	0.769

For a more in-depth explanation on the governing equations, calculation methods and turbulence models, the interested reader is referred to specific CFD literature, like the work of Schlichting [29] or Versteeg and Malalasekera [30].

Boundary Layer Modeling

The averaged governing equations can be reduced to the thin-shear-layer equations which describe the thermo-viscous boundary layer [12,13]. These simplified equations are given by Equations 1a, b, c and are the ones used to determine the wall models.

$$\frac{\partial \bar{\rho}}{\partial t} + \frac{\partial}{\partial x}(\bar{\rho}\bar{u_x}) + \frac{\partial}{\partial y}(\bar{\rho}\bar{u_y}) = 0 \tag{1a}$$

$$\rho\left[\frac{\partial \bar{u_x}}{\partial t} + \bar{u_x}\frac{\partial \bar{u_x}}{\partial x} + \bar{u_y}\frac{\partial \bar{u_x}}{\partial y}\right] = -\frac{\partial \bar{p}}{\partial x} + \frac{\partial}{\partial y}\left[(\bar{\mu} + \mu_t)\frac{\partial \bar{u_x}}{\partial y}\right] \tag{1b}$$

$$\rho c_p\left[\frac{\partial \bar{T}}{\partial t} + \bar{u_x}\frac{\partial \bar{T}}{\partial x} + \bar{u_y}\frac{\partial \bar{T}}{\partial y}\right] = \frac{\partial \bar{p_0}}{\partial t} + \frac{\partial}{\partial y}\left[(\bar{\lambda} + \lambda_t)\frac{\partial \bar{T}}{\partial y}\right] + \dot{Q} \tag{1c}$$

In these equations, the velocity u is split into its components u_x and u_y at the wall. The hydrodynamic pressure gradient is assumed to be independent of the direction normal to the wall, while the thermodynamic pressure p_0 is still related to the ideal gas equation $p_0 = \rho RT$. The viscous stress tensor is replaced by its definition as the product of the dynamic viscosity and the velocity gradient normal to the wall, while the same is applied to the heat flux vector, which can be described as the product of the thermal conductivity and the temperature gradient. In both, the contributions of the turbulence to the viscosity and conductivity has to be taken into account. It is this form of the momentum (1b) and energy (1c) equation that is used to derive the momentum and thermal wall model.

Equilibrium Wall Models

By applying a set of assumptions to Equations 1b and 1c [12], the momentum and energy equation can be reduced to two decoupled ordinary differential equations. These can then be analytically integrated to derive the momentum and thermal wall model. Applying

this procedure to the momentum equation (1b), the well-known universal momentum wall model or law of the wall becomes [12,13,29,30]:

$$u^+ = \begin{cases} y^+ & \text{if} \quad y^+ < 11 \\ \frac{1}{\kappa} ln(y^+) + B & \text{if} \quad y^+ \geq 11 \end{cases} \tag{2}$$

Here u^+ and y^+ are the non-dimensional velocity and wall distance respectively, κ is the von-Kármán constant of 0.41 and B is the log-law constant of 5.2. These non-dimensional parameters are obtained by dividing the velocity u_x and the distance from the wall y by a shear velocity u_τ and a viscous length scale δ_v:

$$u^+ = \frac{u_x}{u_\tau} \qquad y^+ = \frac{y}{\delta_v}$$
$$with \quad u_\tau = \sqrt{\frac{\tau_w}{\rho_w}} \qquad \delta_v = \frac{\nu_w}{u_\tau} \tag{3}$$

where τ_w is the shear stress at the wall $\tau_w = \mu_w \frac{\partial \bar{u}_x}{\partial y}|_w$ and ρ_w, ν_w and μ_w are the respective density, kinematic viscosity and dynamic viscosity at the wall.

A thermal law of the wall can also be derived by simplifying and analytically integrating the energy equation (1c). This integrating procedure is described by Han and Reitz [22]. This method is however less universal [12]. A few different thermal wall models exist resulting from varying simplifications used to derive the analytical solution. Both the transient term and the convection terms on the left hand side of Equation 1c are neglected in all models, which is why they are called equilibrium models. The difference then occurs when determining which terms on the right hand side are discarded and which are retained. They however all have a general appearance, namely a linear and a logarithmic part, which resembles the momentum wall model given in Equation 2. An example of such a thermal law of the wall is the most simple model, derived by Launder and Spalding [20]:

$$T^+ = \begin{cases} Pr\, y^+ & \text{if} \quad y^+ < 11 \\ Pr_t(\frac{1}{\kappa} ln(y^+) + B) + \mathcal{P} & \text{if} \quad y^+ \geq 11 \end{cases}$$
$$with\ \mathcal{P} = Pr_t \frac{\pi/4}{sin(\pi/4)} \left(\frac{A^+}{\kappa}\right)^{\frac{1}{2}} \left(\frac{Pr}{Pr_t} - 1\right) \left(\frac{Pr_t}{Pr}\right)^{\frac{1}{4}} \tag{4}$$

where A^+ is the van Driest constant which has a value of 26 and T^+ is the non-dimensional temperature, derived by subtracting the wall temperature T_w from the temperature T and dividing by the shear temperature T_τ. Together with the relationship between T_τ and the wall heat flux q_w, this heat flux can be calculated.

$$T^+ = \frac{\bar{T} - T_w}{T_\tau}, \qquad T_\tau = \frac{q_w}{\rho_w c_p u_\tau}, \qquad q_w = \lambda_w \frac{\partial \bar{T}}{\partial y}|_w \tag{5}$$

Other thermal wall models exist, which differ from the previous one by maintaining the pressure work term from the energy equation, by accounting for variable density, variable viscosity, … These models are summarized in Table A1, together with the derived calculation for the wall heat flux in Table A2. Important to repeat is that these wall models all neglect the transient and convection terms from the energy equation, to allow an analytical solution to be derived. On the derivation of these thermal wall models, the interested reader is referred to the specific literature [20, 21, 22, 23, 24].

Low Reynolds Turbulence Modeling

By retaining all terms in the momentum (1b) and energy (1c) equation and by accounting for variable density and other transport properties, a non-equilibrium method is obtained, as described by Ma et al. [13]. The equations can then no longer be decoupled and no analytical solution is possible. The wall heat flux can be calculated from its definition in Equation 6, by explicitly solving the temperature profile from Equation 1c.

$$q_w = (\bar{\lambda} + \lambda_t)_w \frac{\partial \bar{T}}{\partial y}|_w \tag{6}$$

It is clear from Equation 6 that this method requires to resolve the temperature accurately in the near-wall region, to allow a correct calculation of the temperature gradient. The complete thermo-viscous boundary layer, for which the structure can be seen in Figure 2, has to be resolved. More specifically, it is important that the thermo-viscous sublayer is accurately resolved, as it is the region closest to the wall. It is in this region that a correct calculation of the temperature gradient is necessary to correctly capture the wall heat flux. It is also in this region that the Reynolds stress is negligible compared to the viscous stress [31]. It is due to this fact that this method of determining the heat flux is called low Reynolds turbulence modeling.

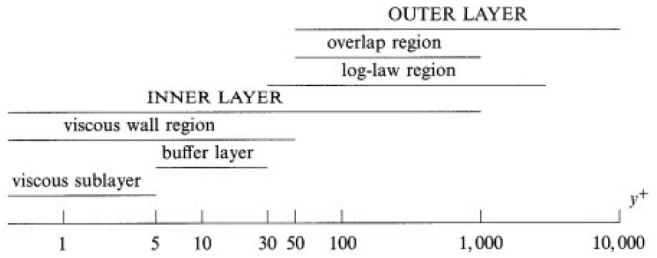

Figure 2. Schematic of the near-wall regions [31]

To resolve these near-wall regions accurately, it is necessary to increase the refinement in the zones close to the wall. Narrow layers have to be added to reduce the y^+-value in these zones. As can be seen in the results section of this paper, wall heat flux values are incorrect when these layers are not added or when they are insufficiently fine.

Computational Mesh

To perform these engine simulations, a computational mesh of the CFR engine is needed. As this is a simple pancake engine, the mesh for the closed cycle simulations was a simple cylinder with cubic cells. Due to symmetry, which can be used in a RANS simulation, the mesh could even be simplified to a 5° wedge with orthogonal cells, which had an aspect ratio of around one. These cells were sufficient when utilizing an equilibrium wall model, however, as said before, when low Reynolds turbulence modeling is applied, fine layers need to be implemented. In Figure 3, a detail at the corner of the cylinder

head and the liner of the mesh used for these types of simulations is displayed. Here one can see the fine layers around the walls, while maintaining the slightly stretched original cells in the center. This refinement in the near-wall region however increased the computational cost, but as the geometry is simple and symmetry could be used, the computation time remained acceptable.

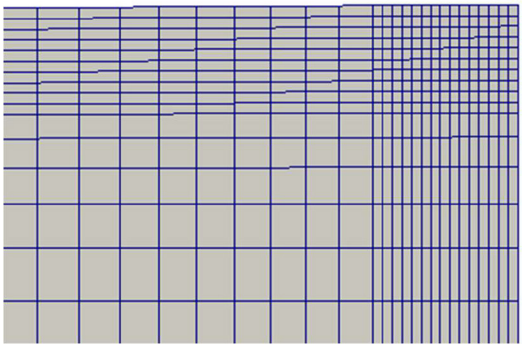

Figure 3. Detailed section of the near-wall region of the mesh used for simulations with low Reynolds turbulence modeling

These closed cycle simulations have the benefit of being fast and numerically less demanding, but they require the flow field to be known and imposed at IVC. One therefore has to rely on flow field measurements, which can be inaccurate, or on assumptions. For the same CFR engine, Rakopoulos et al. assumed a swirl ratio of 1.5 at IVC and imposed this to their simulations [27,28]. To reduce this uncertainty and investigate the influence of the flow field, it was decided to perform full cycle 3D simulations as well and compare results to the ones obtained from the closed cycle simulations. The mesh that was used for these types of calculations can be seen in Figures 4 and 5.

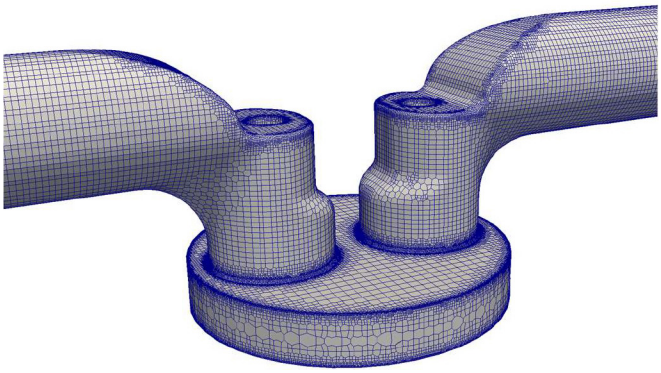

Figure 4. Numerical mesh of the CFR engine, used for the full cycle 3D simulations

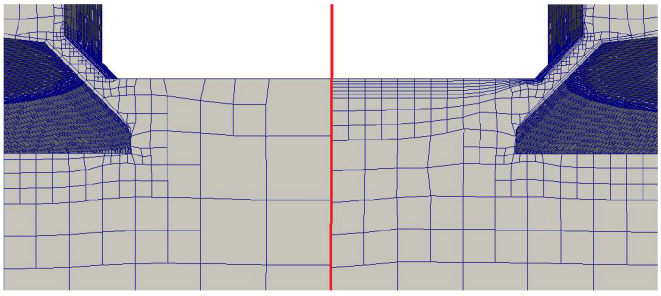

Figure 5. Detail of the full cycle mesh at the cylinder head. Left: no layering added for the simulations with wall functions, right: layers added for the low Reynolds turbulence modeling

Both the approach of using wall models and applying low Reynolds turbulence modeling was also used for these full cycle simulations. Both require however a different grid sizing, as was already mentioned. For the low Reynolds turbulence modeling of the near-wall region, fine layers have to be added, as can be seen in Figure 5. To make this calculation numerically possible, refinement and layering has only been added to the cylinder head. The mesh sizing at other walls remained the same. The small difference this will cause in in-cylinder values for variables such as pressure and temperature (due to not applying the low Reynolds technique at the other walls), was considered acceptable. The total cell count of this mesh therefore resulted to almost 1 million cells, while the simulations using wall functions only require a grid with half a million cells. Applying both methods to these full cycle simulations allowed for a full comparison between both closed and full cycle simulations and the used modeling technique, resulting in a complete comprehensive evaluation.

Results and Discussion

The CFD simulations and heat flux calculations of motored operation of ICEs presented in this research, were all performed using the OpenFOAM® software. A RANS method with standard k-ε turbulence model was used and the wall function models presented in [20, 21, 22, 23, 24] were implemented. Concerning the results, first a validation of the numerical method was performed by comparing numerical results from simulations with the GM engines with results found in [24]. Then the mesh (in)dependency was checked when using the wall function approach or the low Reynolds turbulence modeling.

The latter is a method that is largely dependent on the grid size near the wall. Results are therefore only accurate when they do not change when refining the grid size. This has to be checked to make sure that a correct mesh is used during simulations. Lastly, the extended experimental database of heat flux measurements on the CFR engine was used and compared with different kinds of simulations. This comparison is the main focus of this research as it allowed a full performance evaluation of heat flux calculation approaches.

Validation of Numerical Method

To check the validity of the numerical method, closed cycle simulations of the standard GM and the GM Triptane engine were performed. These are two pancake engines described in [24]. As Rakopoulos et al. [24] already performed a mesh independency test, a similar but slightly more refined grid as theirs was used during these closed cycle simulations. The obtained heat flux results were compared to the ones given by Rakopoulos et al. [24], who did an evaluation of the different wall function models described in [20, 21, 22, 23, 24].

For the GM Triptane engine, operated at a rotational speed of 750 rpm, the heat flux through the cylinder head at 30.22 mm off-center can be seen in Figure 6. The obtained results with different wall functions follows the general trend declared by Nijeweme et al. [8] and Reitz et al. [25] of under-predicting the heat flux. This under-prediction is also found by Rakopoulos et al. [24], albeit to a lesser extent, with even some models correctly capturing the magnitude of the peak wall heat flux. This difference can be caused by various reasons, like for instance a difference in turbulence modeling, tuning

of parameters,… As they use their in-house software, and don't provide a large amount of details on this software, it remains difficult to explain the found differences. However, as the results given in Figure 6 follow the general trend of under-predicting the heat flux with wall functions, this difference was not considered critical. Furthermore, the heat flux graph progress as a function of crank-angle and the relationship between the different wall functions was found to be the same as in [24]. The wall functions described by Rakopoulos et al. [24] and Han and Reitz [22] performed the best, while those developed by Launder and Spalding [20] and Huh et al. [21] performed the worst, exactly as found in [24].

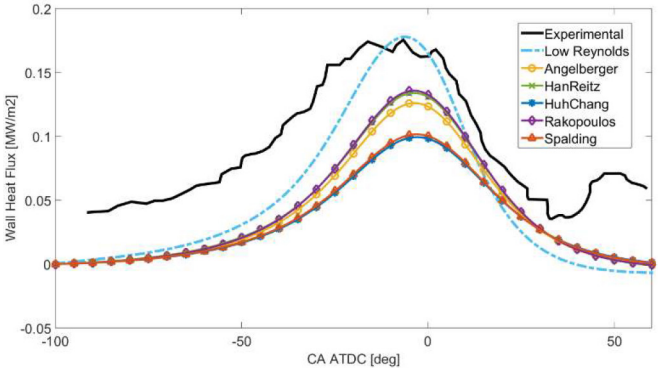

Figure 6. Heat flux simulation results during motored operation of the GM Triptane engine

The same procedure was repeated for the standard GM engine, operating at a rotational speed of 1500 rpm. The heat flux was measured at four different locations in the cylinder head, as described by Alkidas [16]. In Figure A1 of Appendix A, the results on the heat flux can be found. Comparing these with the results presented by Rakopoulos et al. [24], the same findings as before arise. A general under-prediction of the wall heat flux is found when using wall functions, which is to a lesser extent also the case in the work of Rakopoulos et al. [24]. The curve on the heat flux as a function of crank-angle seems accurate, while the performance pecking order of the wall functions was the same as in [24]. Results for both the standard GM and the GM Triptane engine were therefore considered sufficiently correct and the implemented methodology is found adequate.

In Figures 6 and A1, the results from a closed cycle simulation using low Reynolds turbulence modeling can already be seen. It is clear that this approach is superior to the wall function method, as the peak heat flux is correctly predicted, while also predicting an earlier and steeper rise of the heat flux before top dead center and a faster descent afterwards, which is also found in experiments. Discussion on this superior predictive capability is however postponed to later on in this work, when discussing the results on the CFR engine.

Mesh Independency

Before considering the results from simulations as representative, a mesh independency check should be performed for RANS simulations. When applying the wall function approach, a mesh size similar to the one used in [24], where results were found to be independent of further refinements, was used. Even if the sizing was considered appropriate by Rakopoulos et al. [24], a quick mesh independency study was still performed for the CFR engine, by doubling and halving the number of cells. It was found that the results did not significantly change between the various cases, guaranteeing us that our initial mesh was appropriate.

Before considering the low Reynolds turbulence modeling technique as reliable, the mesh quality needs to be assured. As this is a method that resolves the thermo-viscous near-wall region, a sufficiently fine grid sizing near the walls needs to be used. Layers are therefore added around the walls and an example of such a layered grid in the near-wall region can be seen in Figure 3. To check the validity of the mesh, the added layers are gradually refined and an acceptable mesh is found when results no longer change when refining the grid size. This refinement of the grid is indicated with the decreasing value of the y^+-parameter. The results of this mesh independency check, for closed cycle heat flux simulations of the CFR engine, can be seen in Figure 7.

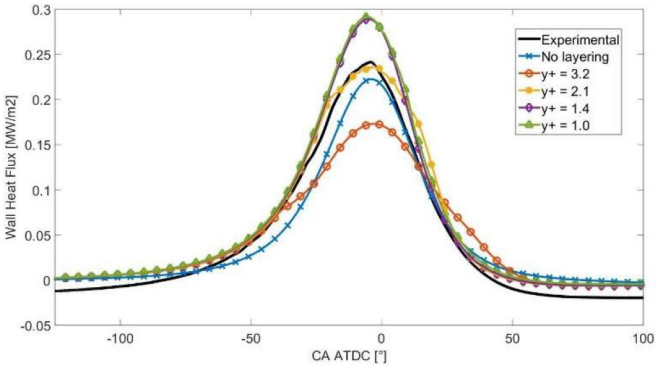

Figure 7. Mesh dependency check for simulations with low Reynolds turbulence modeling

As can be seen in this figure, the change in the prediction of the heat flux stops when decreasing the y^+-value below 1.5. It is therefore clear that a sufficiently fine near-wall grid sizing should be used, to achieve a y^+ below 1.5, guaranteeing a correct use of the low Reynolds turbulence modeling and a correct prediction of the related heat flux. For the CFR engine, the grid that resulted in a y^+-value of 1.4 was used for the closed cycle simulations. Here sufficiently fine layers were added at all walls. The same sizing was applied to the geometries for the standard GM and the GM Triptane engine, for which heat flux results using the low Reynolds turbulence modeling could already be seen in Figures 6 and A1. To lighten the computational load of the full cycle simulations of the CFR engine, layers were only added at the cylinder head and the low Reynolds turbulence modeling technique was only applied to that region. A y^+-value of 1.1 was found at the cylinder head, which was deemed to be sufficient.

Results and Performance Evaluation

For the closed cycle simulations of the CFR engine, both the wall function and the low Reynolds approaches were applied. The compression ratio was varied between 9, 10 and 11 and the wall heat flux was calculated at the position P1 in the cylinder head and P2 in the liner. For this last position, only results from operation with a compression ratio of 10 were studied, as this was the only case for which experimental heat flux measurements at the liner were available. A comparison between the different methods was performed, with the aid of experimental data and the graphs given in Figures 8 and 9.

From Figure 8, it is clear that the wall function method is incapable of correctly predicting the wall heat flux at the cylinder head. For all studied compression ratios, all wall models under-predict the heat flux. Even the best performing ones - those developed by Rakopoulos et al. [24] and Han and Reitz [22] - still have a 20 to 25% under-prediction of the peak heat flux. Furthermore, these wall models are not able to predict the heat flux trends as a function of crank angle that were found in experiments. They predict a too late rise in heat flux, as the climb in heat flux is registered starting at 50 °CA BTDC, while experiments indicate that this should start around 75 °CA BTDC. A too slow descent of the wall heat flux is also found after top dead center. Experiments indicate a fast descent in the measured heat flux at the cylinder head which ends at 50 °CA ATDC, while simulations using the wall functions predict an end at 70 °CA ATDC. When comparing simulations to experiments, a slight shift to the right in the graphs is also noted, for the moment when the peak heat flux is reached. This last difference however can be neglected as the difference is small and not significant.

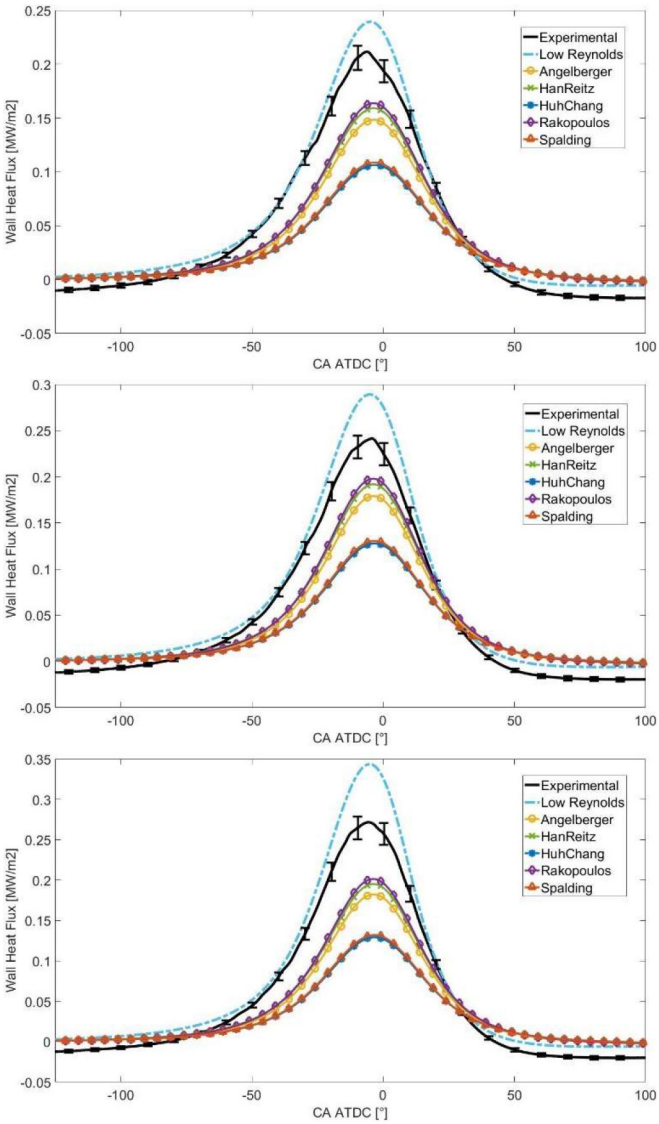

Figure 8. Heat flux results from the closed cycle simulations and from experiments at the sensor location P1 (cylinder head) of the CFR engine. Top: CR = 9, Middle: CR = 10, Bottom: CR = 11

The same conclusions can be drawn by studying the heat flux at the liner, given in Figure 9 for the CFR engine operating at a compression ratio of 10. Both an under-prediction of the peak heat flux and an incorrect heat flux trend as a function of crank angle are found, when comparing wall function simulations with experiments. These findings indicate that not all occurring effects inside the engine can be captured by this wall function approach. They necessitate the use of a different approach and confirm the idea posted by Ma et al. [12,13] that a non-equilibrium or low Reynold turbulence modeling approach is necessary to accurately calculate the wall heat flux.

Resolving the thermo-viscous boundary layer by applying low Reynolds turbulence modeling to the walls of the closed cycle simulations and calculating the heat flux accordingly, was also performed. Results of this type of simulation for the CFR engine are represented by the blue dash-dotted line seen in Figures 8 and 9. From Figure 8, representing the heat flux at the sensor location P1 in the cylinder head, it is clear that this method is superior to the wall function modeling. For all compression ratios, the predicted heat flux curve follows the same trends as the experimental results, with a correct prediction of the start and end of heat flux rise and descent, and only an over-prediction of the peak heat flux as a disadvantage. This disadvantage is however not found when looking at Figure 9, where the heat flux at the sensor location P2 in the liner is depicted. The peak heat flux is almost correctly predicted and numerical and experimental results, given by the blue dash-dotted and the black full line, almost perfectly coincide, especially when considering the error margin on the measurements. This clearly illustrates the better predictive capabilities of the low Reynolds turbulence modeling approach concerning the heat flux through the engine walls and its capability to capture all occurring effects. As the calculation time only increased from 20 processor-minutes for the wall function simulations to 150 processor-minutes for the simulations using the low Reynolds formulations, it was concluded that for closed cycle simulations, the calculation time remained acceptable and that the low Reynolds formulation is superior to the wall function one.

This benefit of using low Reynolds turbulence modeling at the wall and resolving the thermo-viscous boundary layer is also illustrated in Figures 6 and A1 for the GM Triptane and the standard GM engine respectively. The calculated peak heat flux is accurate compared to experimental measurements, and the progress of the heat flux as a function of crank angle is better compared to the wall function approach. This is especially true for the standard GM engine, where the curve representing the numerical results also follows the experimental measurements.

One thing to note however, as already stated above, is an over-prediction of the peak heat flux at the cylinder head, whereas the heat flux at the liner is almost perfectly captured. A possible explanation for this phenomenon is the applied wall temperature during simulations. To maintain simplicity, a constant wall temperature, which was based on the value of the cooling water, was implemented at all walls. For the case with a compression ratio of 10, this temperature had a value of 382 K. It is however highly unlikely that all walls experience the same temperature. Furthermore, the fact that the wall temperature was set constant is also a large simplification. When changing the implemented wall temperature for the cylinder head to 432 K, but maintaining the value of 382 K for the liner, results improve, as can be seen in Figure 10. The curve representing

the heat flux measured at the location P1 in the cylinder head more closely approaches the experimental curve, with especially a more accurate peak heat flux. The measured heat flux at the liner on the other hand does not change, maintaining its large coincidence with experimental results. The general prediction therefore improves, with both the heat flux at sensor location P1 in the cylinder head and at P2 in the liner accurately captured.

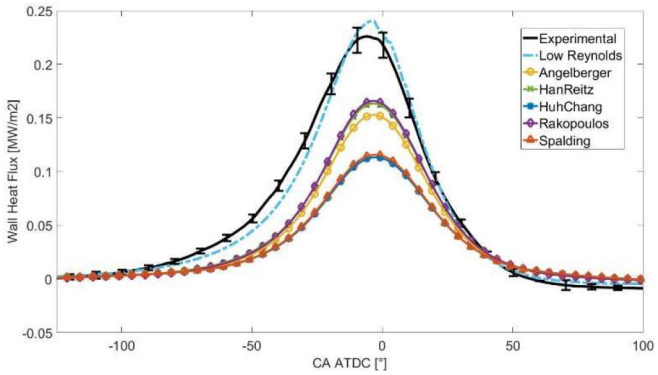

Figure 9. Heat flux results from the closed cycle simulations and from experiments at the sensor location P2 (liner) of the CFR engine, for a compression ratio of 10.

The authors realize that this change in the wall temperature is a large assumption and that no foundation is proposed for the choice of the increased wall temperature at the cylinder head. Figure 10 however only serves as an indication, that with more accurate wall temperatures, a better prediction of the heat flux should be achieved. Further research needs to be conducted, to optimize the simulation strategies, where possible RTD measurements can be used to implement more accurate wall temperatures. Nevertheless, the results presented in Figures 8, 9 and 10 demonstrate the improved predictive capability when using the low Reynolds turbulence model.

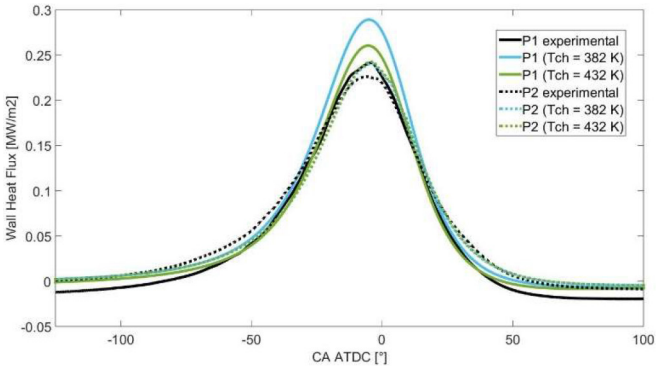

Figure 10. Heat flux results at the sensor location P1 of the CFR engine, with varying wall temperature at the cylinder head

From Figures 8 and 9 it became clear that the wall functions are not able to correctly capture the heat flux, while the low Reynolds turbulence model is. To make sure that this is not due to the assumed flow field at IVC, full cycle simulations with the different methods were also carried out. As a good initialization based on experimental results was used, and RANS simulations were performed, where the interest was in the mean flow field and other variables, a simulation of a single cycle of 720 °CA was deemed to be sufficient. This was supported by the good agreement that was found between numerical and experimental in-cylinder pressure traces.

It was stated that for the closed cycle simulations of the CFR, a swirling flow with a swirl ratio of 1.5 was implemented at intake valve closing, the start of the simulation. This is however a major assumption as nothing is known about the flow field of the CFR engine. To remove this uncertainty and investigate the influence of the flow field, full cycle simulations were performed. From these type of simulations, a swirl ratio of 0.5 at IVC was found. Closed cycle simulations were repeated with this value, but, as this only slightly differs from the previously used value of 1.5, the found differences in results between the two were small. The closed cycle simulations imposing a swirl ratio of 1.5 at IVC were therefore considered adequate and representative to be used in the heat flux analysis.

The possible improvement of heat flux results when using a correct flow field was investigated. The calculated heat flux at sensor location P1, for a compression ratio of 10, is given in Figure 11.

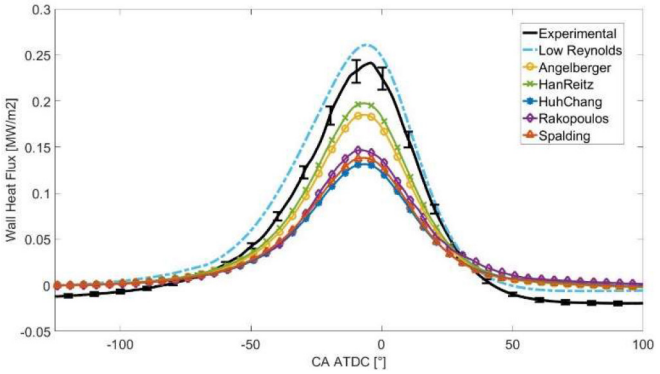

Figure 11. Heat flux results from the full cycle simulations and from experiments at the sensor location P1 (cylinder head) of the CFR engine, for a compression ratio of 10.

Figure 11 shows the results obtained when implementing the various wall functions and when applying the low Reynolds turbulence modeling technique. From this figure it is again clear that the wall functions are not able to correctly capture the heat flux. Furthermore, when using a wall function, no improvement is found between the closed cycle simulation and this full cycle simulation, while the computation does increase to 800 processor-hours. When using the low Reynolds turbulence model on the other hand and resolving the thermo-viscous boundary layer near the cylinder head, accurate heat flux results are found. Results are now even slightly better than those found for the closed cycle simulation. For these full cycle simulations, also a wall temperature of 382 K was implemented, but the curve representing the experimental results is now more accurately followed by the numerical results. This slight improvement however comes at the cost of a large increase in numerical expenses. When only applying grid refinement and the low Reynolds formulation at one wall, calculation time increased to 1500 processor-hours. For heat flux calculations, one is therefore required to make the consideration between a fast and accurate solution and a slow but almost perfect prediction of the heat flux.

Summary and conclusions

The present work details a study of the heat flux through the walls of an internal combustion engine, under motoring operation. Different numerical methods have been used and compared to give a complete overview of the available wall heat flux calculation possibilities. The

availability of an extended database of accurate heat flux measurements on a research CFR engine allowed the performance of all methods to be evaluated.

It was found that no wall function was able to correctly predict the heat flux through the walls of an engine. All of them under-predicted the peak heat flux and the experimentally found trends in the heat flux as a function of crank angle could not be replicated by the simulations. Even by performing full cycle simulations and removing the uncertainty on the flow field, results did not improve. It is clear that, by implementing the simplifications necessary to analytically derive these wall functions, not all effects inside the engine can be captured.

On the other hand, when no simplifications were implemented and the complete thermo-viscous boundary layer was resolved, the heat flux was more accurately predicted. Experimentally found trends were captured effectively while the peak heat flux was also predicted within an acceptable range. The use of full cycle simulations resulted in a slight improvement, but due to the additional numerical cost, these type of simulations are not considered beneficial. Concerning heat flux simulations, closed cycle simulations are deemed to be sufficient, as long as an acceptable assumption can be made when the flow field at IVC is not known. The slight increase in calculation time when performing closed cycle simulations using a low Reynolds turbulence model is accepted, as results are far superior to the ones obtained when using wall functions. It is the authors' opinion that future research on this method should be performed, by for example implementing more accurate boundary conditions, to optimize this simulation strategy and achieve even better results.

References

1. Dec, J.E., "Advanced compression-ignition engines - understanding the in-cylinder processes," *Proceedings of the Combustion Institute*, 32(2):2727-2742, 2009, doi:10.1016/j.proci.2008.08.008
2. Yamakawa, M., Youso, T., Fujikawa, T., Nishimoto, T. et al., "Combustion Technology Development for a High Compression Ratio SI Engine," *SAE Int. J. Fuels Lubr.* 5(1):98-105, 2012, doi:10.4271/2011-01-1871.
3. Broekaert, S., De Cuyper, T., Chana, K., De Paepe, M. et al., "Assessment of Empirical Heat Transfer Models for a CFR Engine Operated in HCCI Mode," SAE Technical Paper 2015-01-1750, 2015, doi:10.4271/2015-01-1750.
4. Broekaert, S., De Cuyper, T., De Paepe, M., and Verhelst, S., "Experimental investigation of the effect of engine settings on the wall heat flux during HCCI combustion," *Energy* 116(1):1077-1086, 2016, doi:10.1016/j.energy.2016.10.042
5. De Cuyper, T., Fossaert, G., Collet, O., Broekaert, S. et al., "Calibration of a TFG Sensor for Heat Flux Measurements in a S.I. Engine," *SAE Int. J. Engines* 8(4):1692-1700, 2015, doi:10.4271/2015-01-1645.
6. De Cuyper, T., Bracke, S., Lavens, J., Broekaert, S. et al., "Demonstrating the Use of Thin Film Gauges for Heat Flux Measurements in ICEs: Measurements on an Inlet Valve in Motored Operation," SAE Technical Paper 2016-01-0641, 2016, doi:10.4271/2016-01-0641.
7. Borman, G., and Nishiwaki, K., "Internal-Combustion Engine Heat-Transfer," *Progress in Energy and Combustion Science*, 11(4):1-46, 1987, doi:10.1016/0360-1285(87)90005-0
8. Oude Nijeweme, D.J., Kok, J.B.W., Stone, C.R., and Wyszynski, L., "Unsteady in-cylinder heat transfer in a spark ignition engine: experiments and modelling," *Proceedings of the Institution of Mechanical Engineers, Part D: Journal of Automobile Engineering* 215(6): 747-760, 2001, doi:10.1243/0954407011528329
9. De Cuyper, T., Chana, K., De Paepe, M., and Verhelst, S., "Heat transfer modelling in spark ignition engines: optimization and instrumentation of a TFG sensor," *Journées d'Étude*, 2014.
10. Koehler, M., Hess, D., and Brücker, C., "Flying PIV measurements in a 4-valve IC engine water analogue to characterize the near-wall flow evolution," *Measurement Science and Technology* 26(12):125302, 2015, doi:10.1088/0957-0233/26/12/125302
11. Müller, S.H.R., Böhm, B., Gleißner, M., Grzeszik, R. et al., "Flow field measurements in an optically accessible, direct-injection spray-guided internal combustion engine using high-speed PIV," *Experiments in fluids* 48(2):281-290, 2010, doi:10.1007/s00348-009-0742-2
12. Ma, P.C., Ewan, T., Jainski, C., Lu, L. et al., "Development and Analysis of Wall Models for Internal Combustion Engine Simulations Using High-speed Micro-PIV Measurements," *Flow, Turbulence and Combustion* 98(1):283-309, 2017, doi:10.1007/s10494-016-9734-5
13. Ma, P.C., Greene, M., Sick, V., and Ihme, M., "Non-equilibrium wall-modeling for internal combustion engine simulations with wall heat transfer," *International Journal of Engine Research*: 1468087416686699, 2017, doi:10.1177/1468087416686699
14. Annand, W.J.D., "Heat transfer in the cylinders of reciprocating internal combustion engines," *Proceedings of the Institution of Mechanical Engineers* 177(1):973-996, 1963, doi:10.1243/PIME_PROC_1963_177_069_02
15. Woschni, G., "A Universally Applicable Equation for the Instantaneous Heat Transfer Coefficient in the Internal Combustion Engine," SAE Technical Paper 670931, 1967, doi:10.4271/670931
16. Alkidas, A.C., "Heat transfer characteristics of a spark-ignition engine." *Journal of Heat Transfer* 102(2):189-193, 1980, doi:10.1115/1.3244258
17. Alkidas, A., Puzinauskas, P., and Peterson, R., "Combustion and Heat Transfer Studies in a Spark-Ignited Multivalve Optical Engine," SAE Technical Paper 900353, 1990, doi:10.4271/900353.
18. Chang, J., Güralp, O., Filipi, Z., Assanis, D. et al., "New Heat Transfer Correlation for an HCCI Engine Derived from Measurements of Instantaneous Surface Heat Flux," SAE Technical Paper 2004-01-2996, 2004, doi:10.4271/2004-01-2996.
19. Hensel, S., Sarikoc, F., Schumann, F., Kubach, H. et al., "Investigations on the Heat Transfer in HCCI Gasoline Engines," *SAE Int. J. Engines* 2(1):1601-1616, 2009, doi:10.4271/2009-01-1804.

20. Launder, B.E., and Spalding, D.B., "The numerical computation of turbulent flows," *Computer methods in applied mechanics and engineering* 3(2): 269-289, 1974, doi:10.1016/0045-7825(74)90029-2
21. Huh, K., Chang, I., and Martin, J., "A Comparison of Boundary Layer Treatments for Heat Transfer in IC Engines," SAE Technical Paper 900252, 1990, doi:10.4271/900252.
22. Han, Z., and Reitz, R.D., "A temperature wall function formulation for variable-density turbulent flows with application to engine convective heat transfer modeling." *International journal of heat and mass transfer* 40(3): 613-625, 1997, doi:10.1016/0017-9310(96)00117-2
23. Angelberger, C., Poinsot, T., and Delhay, B., "Improving Near-Wall Combustion and Wall Heat Transfer Modeling in SI Engine Computations," SAE Technical Paper 972881, 1997, doi:10.4271/972881.
24. Rakopoulos, C.D., Kosmadakis, G.M., and Pariotis, E.G., "Critical evaluation of current heat transfer models used in CFD in-cylinder engine simulations and establishment of a comprehensive wall-function formulation," *Applied Energy* 87(5):1612-1630, 2010, doi:10.1016/j.apenergy.2009.09.029
25. Reitz, R., "Assessment of Wall Heat Transfer Models for Premixed-Charge Engine Combustion Computations," SAE Technical Paper 910267, 1991, doi:10.4271/910267.
26. Ikegami, M., Kidoguchi, Y., and Nishiwaki, K., "A Multidimensional Model Prediction of Heat Transfer in Non-Fired Engines," SAE Technical Paper 860467, 1986, doi:10.4271/860467.
27. Rakopoulos, C.D., Kosmadakis, G.M., and Pariotis,E.G., "Evaluation of a combustion model for the simulation of hydrogen spark-ignition engines using a CFD code," *International Journal of Hydrogen Energy* 35(22):12545-12560, 2010, doi:10.1016/j.ijhydene.2010.09.002
28. Rakopoulos, C.D., Kosmadakis, G.M., Demuynck, J., De Paepe, M. et al., "A combined experimental and numerical study of thermal processes, performance and nitric oxide emissions in a hydrogen-fueled spark-ignition engine," *International Journal of Hydrogen Energy* 36(8):5163-5180, 2011, doi:10.1016/j.ijhydene.2011.01.103
29. Schlichting, H., Gersten, K., Krause, E. and Oertel, H., "Boundary-layer theory, Seventh Edition," (New York: McGraw-hill, 1960), ISBN:978-3-662-52917-1
30. Versteeg, H.K., and Malalasekera, W., "An introduction to computational fluid dynamics: the finite volume method," (Pearson Education, 2007), ISBN:978-0-13-1274983
31. Merci, B., "Modelling of Turbulence and Combustion," (Course at Ghent University, 2015)

Contact Information

Corresponding author:

Gilles Decan
gilles.decan@ugent.be

Acknowledgments

First of all, I want to thank Politecnico di Milano and especially prof. Tommaso Lucchini for their hospitality and the chance they gave me to do a research stay at the ICE group of the Department of Energy. Secondly, I want to thank the *"Fonds Wetenschappelijk Onderzoek Vlaanderen"* for the funding they provided, which made this research stay possible. The complete Ph.D. research is funded by Ghent University (Belgium) through GOA project BOF16/GOA/004.

Definitions/Abbreviations

ABDC - After Bottom Dead Center

ATDC - After Top Dead Center

BBDC - Before Bottom Dead Center

BTDC - Before Top Dead Center

CAD - Crank Angle Degree

CFD - Computational Fluid Dynamics

CFR - Cooperative Fuel Research

DNS - Direct Numerical Simulation

EVC - Exhaust Valve Closing

EVO - Exhaust Valve Opening

HCCI - Homogeneous Charge Compression Ignition

HFM - Hot Film Air Mass

ICE - Internal Combustion engine

VC - Inlet Valve Closing

IVO - Inlet Valve Opening

LES - Large Eddy Simulation

PIV - Particle Image Velocimetry

RANS - Reynolds Averaged Navier-Stokes

RNG - Re-Normalization Group

RTD - Resistance Temperature Detector

SST - Shear Stress Transport

TFG - Thin Film Gauge

$\mathbf{c_p}$ - Specific heat capacity under constant pressure (J kg^{-1} K^{-1})

$\boldsymbol{\delta_v}$ - Viscous length scale (m)

$\boldsymbol{\lambda}$ - Thermal conductivity (W m_{-1} K^{-1})

$\boldsymbol{\lambda_t}$ - Turbulent thermal conductivity (W m^{-1} K^{-1})

$\boldsymbol{\mu}$ - Dynamic viscosity (Pa s)

$\boldsymbol{\mu_t}$ - Turbulent dynamic viscosity (Pa s)

$\boldsymbol{\nu}$ - Kinematic viscosity (m^2 s^{-1})

p - Hydrodynamic pressure (Pa)

$\mathbf{p_0}$ - Thermodynamic pressure (Pa)

Pr - Prandtl number

$\mathbf{Pr_t}$ - Turbulent Prandtl number

$\boldsymbol{\rho}$ - Density (kg m^{-3})

q - Heat flux vector (W m^{-2})

$\mathbf{q_t}$ - Turbulent heat flux vector (W m^{-2})

$\dot{\boldsymbol{Q}}$ - Source term for the rate of heat release (W m^{-3})

R - Universal gas constant (J kg^{-1} K^{-1})

T - Temperature (K)

$\mathbf{T}_{\tau}$ - Shear temperature (K)

$\boldsymbol{T}^{+}$ - Non-dimensional temperature (-)

τ - Viscous stress tensor (Pa)

$\boldsymbol{\tau}^{t}$ - Turbulent viscous stress tensor (Pa)

u - Velocity flow field (m s^{-1})

$\mathbf{u}^{\tau}$ - Shear velocity (m s^{-1})

$\mathbf{u}^{x}$ - Velocity along the x-axis (m s^{-1})

$\mathbf{u}^{y}$ - Velocity along the y-axis (m s^{-1})

$\boldsymbol{u}^{+}$ - Non-dimensional velocity parallel to the wall (-)

y - Distance from the wall (m)

$\boldsymbol{y}^{+}$ - Non-dimensional distance from the wall (-)

APPENDIX

In this appendix, graphs and figures which did not fit the page layout in the main body of the paper are added. They are referred to throughout the paper content.

Table A1. Different thermal wall models

Model	Temperature profile	Valid y^+	T^+
Launder and Spalding [20]	$T^+ = Pr\, y^+$	$y^+ < 11$	$T^+ = \frac{\rho c_p u_\tau (T_w - T)}{q_w}$
	$T^+ = Pr_t(\frac{1}{\kappa} ln(y^+) + B)) + \mathcal{P}$	$y^+ \geq 11$	
Angelberger et al. [23]	$T^+ = Pr\, y^+$	$y^+ < 11$	$T^+ = \frac{\rho c_p u_\tau T}{q_w} ln(\frac{T_w}{T})$
	$T^+ = Pr_t(\frac{1}{\kappa} ln(y^+) + B)) + \mathcal{P}$	$y^+ \geq 11$	
Han and Reitz [22]	$T^+ = 2.1\, ln(y^+) + 2.5$	$All\ y^+$	$T^+ = \frac{\rho c_p u_\tau T}{q_w} ln(\frac{T_w}{T})$
Huh et al. [21]	$T^+ = Pr\, y^+ - 0.5 Pr S^+ (y^+)^2$	$y^+ < 11$	$T^+ = \frac{\rho c_p u_\tau (T_w - T)}{q_w}$
	$T^+ = 13.2Pr + 2.195\, ln(y^+) - 5.66\ -\ \ldots$ $-\ S^+(87.12Pr + 2.195\, y^+ - 28.98)$	$y^+ \geq 11$	
Rakopoulos et al. [24]	$T^+ = \frac{1}{0.4767}\left[ln\left(y^+ + \frac{1}{0.4767Pr}\right) - ln\left(40 + \frac{1}{0.4767Pr}\right)\right] + \ldots$ $+ 10.2384 + P^+\left(\frac{y^+ - 40 + 117.31(0.4767 + \frac{1}{Pr})}{0.4767 + \frac{1}{Pr}}\right)$	$All\ y^+$	$T^+ = \frac{\rho c_p u_\tau T}{q_w} ln(\frac{T_w}{T})$

Table A2. Wall heat flux for the various equilibrium models

Model	Wall heat flux	y^+ valid
Launder and Spalding [20]	$q_w = \frac{\rho c_p u_\tau (T_w - T)}{Pr\, y^+}$	$y^+ < 11$
	$q_w = \frac{\rho c_p u_\tau (T_w - T)}{Pr(\frac{1}{\kappa} ln(y^+) + B) + \mathcal{P}}$	$y^+ \geq 11$
Angelberger et al. [23]	$q_w = \frac{\rho c_p u_\tau T\, ln(T_w/T)}{Pr\, y^+}$	$y^+ < 11$
	$q_w = \frac{\rho c_p u_\tau T\, ln(T_w/T)}{Pr(\frac{1}{\kappa} ln(y^+) + B) + \mathcal{P}}$	$y^+ \geq 11$
Han and Reitz [22]	$q_w = \frac{\rho c_p u_\tau T\, ln(T_w/T)}{2.1\, ln(y^+) + 2.5}$	$All\ y^+$
Huh et al. [21]	$q_w = \frac{\rho c_p u_\tau (T_w - T) - 0.5 Pr \frac{dP}{dt} \frac{\nu}{u_\tau} (y^+)^2}{Pr\, y^+}$	$y^+ < 11$
	$q_w = \frac{\rho c_p u_\tau (T_w - T) - \frac{dP}{dt} \frac{\nu}{u_\tau} (87.12Pr + 2.195\, y^+ - 28.98)}{13.2Pr + 2.195\, ln(y^+) - 5.66}$	$y^+ \geq 11$
Rakopoulos et al. [24]	$q_w = \frac{\rho c_p u_\tau T\, ln(T_w/T) - \frac{dP}{dt} \frac{\nu}{u_\tau} \left(\frac{y^+ - 40}{0.4767 + \frac{1}{Pr}} + 117.31\right)}{\frac{1}{0.4767}\left[ln(y^+ + \frac{1}{0.4767Pr}) - ln(40 + \frac{1}{0.4767Pr})\right] + 10.2384}$	$All\ y^+$

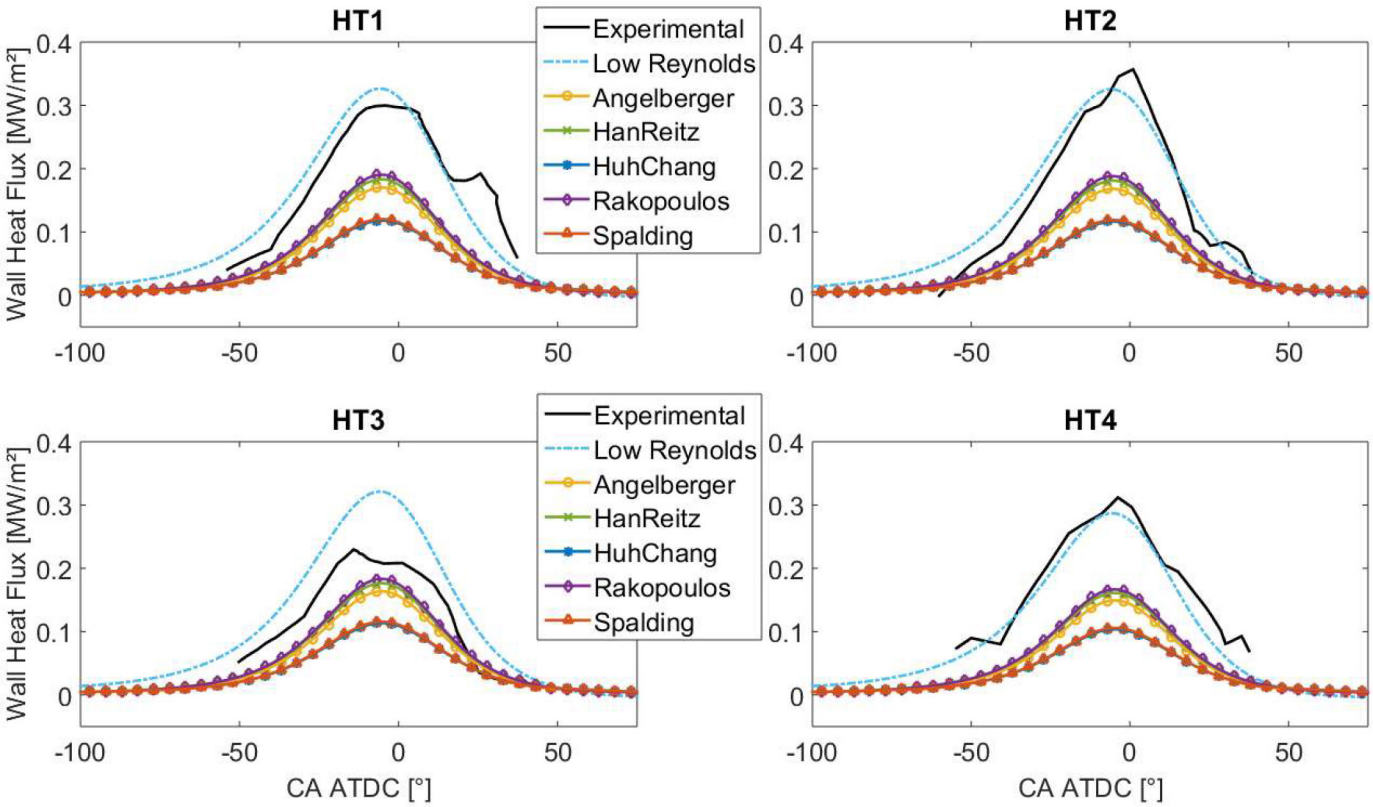

Figure A1. Heat flux simulation results at various sensor locations, during motored operation of the standard GM engine.

ISSN 0148-7191

http://papers.sae.org/2017-24-0032